Earth Planet. Sci. Lett. 629 (2024) 118593

Contents lists available at ScienceDirect

Earth and Planetary Science Letters

journal homepage: www.elsevier.com/locate/epsl

Spatio-temporal evolution of rift volcanism controlled top-down by a deepening graben

Gaetano Ferrante [a,b,*], Eleonora Rivalta [a,c], Francesco Maccaferri [d]

[a] Dipartimento di Fisica e Astronomia, Alma Mater Studiorum - Università di Bologna, Viale Berti Pichat, 8, Bologna, 40126, Italy
[b] Department of Earth, Environmental and Planetary Sciences, Rice University, 6100 Main Street, Houston, 77005, TX, USA
[c] Helmholtz Centre Potsdam GFZ German Research Centre for Geosciences, Telegrafenberg, Potsdam, 14473, Germany
[d] Istituto Nazionale di Geofisica e Vulcanologia (INGV), Osservatorio Vesuviano, Napoli, 80124, Italy

ARTICLE INFO

Editor: R. Bendick

Keywords:
rift magmatism
dike propagation
sill emplacement
surface loading
elastic stresses

ABSTRACT

Volcanism in continental rifts is generally observed to shift over time from the inside of the basin to its flanks and vice versa, but the controls on these switches are still unclear. Here we use numerical simulations of dike propagation to test the hypothesis that the spatio-temporal evolution of rift volcanism is controlled by the crustal stresses produced during the development of the rift basin. We find that the progressive deepening of a rift rotates the direction of the principal stresses under the basin, deflecting ascending dikes. This causes an early shift of volcanism from the inside of the graben to its flanks. The intensification of this stress pattern, due to further deepening of the basin, promotes the formation of lower crustal sill-like intrusions that can stack under the rift, shallowing the depth at which dikes nucleate, eventually causing a late stage of in-rift axial volcanism. Given the agreement between our model results and observations, we conclude that the temporal shifts in the location of rift volcanism are controlled to first order by the elastic stresses developing in the crust as the rift matures. We thereby suggest that geodynamic models should account for elasticity and the redistribution of surface loads in order to effectively reproduce rift-related magmatism.

1. Introduction

Continental rifting is the process by which the continental lithosphere is slowly thinned and deformed over timescales of millions of years, in response to extensional forces of different origin that result in the formation of large scale fault-bounded basins. Over such time scales, the weakest layers of the lithosphere are expected to behave viscously. Consequently, numerical models of rifting usually assume visco-elasto-plastic rheologies for the lithosphere. While geodynamic models effectively reproduce the deformation history of rifts, they usually fail to capture the behavior of another fundamental feature of rifted areas, that is the evolution of magmatism. Indeed, continental rifting is often accompanied by volcanism (White, 1992), whose location is observed to shift during a rift's lifetime. In particular, volcanism often migrates from the inside of the rift graben (in-rift volcanism) to its flanks (off-rift volcanism) during the early stages of rifting, and then back to the axial portion during rift maturity. These patterns are commonly observed regardless of the underlying cause of rifting or whether the rift is magma-rich or magma-poor, suggesting a common control, despite the differences between individual rifts and their specific complexities. However, in spite of the recent advances, the mechanisms governing the spatio-temporal evolution of rift magmatism are still poorly understood. The shifts in the loci of magmatic activity in rifts have often been explained in terms of their tectonic evolution, but the models advocated are usually ad-hoc and thus unable to capture the ubiquity of the observed patterns. A comprehensive model of rift magmatism needs to explain why rifts of very different nature and complexity share the following overarching observations: i) the temporal shifts in the location of eruptive vents (e.g. Michon and Merle, 2001; Liu et al., 2001; Corti, 2009), ii) the accumulation at depth of large magma volumes through the emplacement of multiple sill-like intrusions (Thybo and Nielsen, 2009; Thybo and Artemieva, 2013), iii) why the shifts from pattern to pattern occur relatively abruptly if compared to the overall duration of volcanism, marking well-defined 'phases', iv) and the fact that different phases of volcanism are often associated with differences in magma composition (Pasteels et al., 1989).

While no model so far has achieved an overarching explanation of the spatio-temporal and geochemical patterns described above, there

* Corresponding author.
E-mail address: gaetano.ferrante@studio.unibo.it (G. Ferrante).

https://doi.org/10.1016/j.epsl.2024.118593
Received 23 September 2023; Received in revised form 13 December 2023; Accepted 23 January 2024
Available online 31 January 2024
0012-821X/© 2024 Elsevier B.V. All rights reserved.

have been attempts to explain some of the observed shifts, with many authors focusing on the counterintuitive locations of off-rift volcanoes. Some studies attributed the occurrence of flank volcanism to the interaction of magma with boundary faults (e.g. Bosworth, 1987; Corti et al., 2004). Bosworth (1987) ascribed the existence of off-rift volcanoes to the presence of low-angle detachment faults beneath asymmetric rifts, that would tap the asthenosphere and weaken the crust, facilitating magma migration far from the basin. Corti et al. (2004) used analogue models to propose that surface deformation controls the migration of magma towards the footwall of the boundary faults, that would in turn channel magma to the surface to feed off-rift volcanoes. However, these interpretations are not fully supported by independent observations for a number of reasons: in particular, there is little to no evidence of deeply penetrating detachment faults underlying extensional areas (Ellis and King, 1991) and propagation of magma along faults is now considered to be a minor mechanism (Pollard, 1987; Ziv et al., 2000). It is increasingly recognized that, in all tectonic contexts, the overarching control on magma pathways lies in the elastic stresses acting in the lithosphere (Anderson, 1937; Muller and Pollard, 1977; Rubin, 1995; Rivalta et al., 2015). Regardless of the mechanisms driving rifting and the production of melt in the mantle, once magma reaches the lithosphere its ascent pathways will be controlled by elastic stresses. In fact, magma transport through the lithosphere occurs mostly through diking, a form of hydraulic fracturing (e.g. Rubin, 1995). As predominantly opening fractures, dikes tend to open roughly in the direction of least compression, rather than follow directions optimally oriented for shearing, which would not accommodate efficiently the intruded magma (e.g. Anderson, 1937; Weertman, 1971; Nakamura, 1977; Muller and Pollard, 1977; Pollard, 1987; Dahm, 2000; Ziv et al., 2000; Watanabe et al., 2002).

Ellis and King (1991) suggested that flank volcanism in continental rifts could be explained by the dilational strain caused at the base of the footwall by faulting in a flexurally supported crust, which would favor upward magma propagation provided that melt is available in the lower crust. Maccaferri et al. (2014) proposed to include the unloading stresses induced by the formation of the rift graben in the stress computations. They built a zero-order stress model by superposing a negative strip load (simulating the surface mass load missing in correspondence of the basin) to a uniform stretching of the lithosphere. They then used a dike propagation code (Maccaferri et al., 2010, 2011) based on the principles of linear fracture mechanics (Griffith, 1921; Dahm, 2000) to simulate magma ascent in such a 'gravitationally unloaded', extending rift. Their model predicts that when the stresses due to the unloading of the graben dominate over the tectonic tension, the direction of least compression becomes vertical in a depth range under the basin, turning ascending dikes into subhorizontal magma bodies or forcing their way up to the rift flanks on oblique trajectories.

Here, we further test the Maccaferri et al. (2014) model against its ability to predict the shifting through time of vent locations in rifts, along with the overarching observations listed above, solely on the basis of the evolution of unloading forces due to the deepening of the graben. To do so, we further develop the modeling approach of Maccaferri et al. (2014) so that it accounts for time-dependent stresses by including the following elements in the model: a) time-dependent unloading due to a deepening graben subjected to sedimentation, b) stress interaction between successive dike intrusions. We focus most of our numerical simulations to the case of a full-graben. In addition, our study extends to the case of a half-graben, in order to investigate whether the asymmetric distribution of volcanism observed in many half-grabens (Janecke et al., 1997; Bjorklund et al., 2002) can be explained in terms of the stresses generated in the crust by an asymmetric graben.

With the purpose of developing a widely applicable idealized rifting model, we keep the geometries simple and choose parameters of general relevance. While inevitably resulting in decreased ability to match the complexity of specific rift settings, this may promote a clearer understanding of the major mechanisms controlling the spatio-temporal evolution of rift volcanism. This would clarify the controls on several processes of global relevance, such as underplating, the evolution of crustal rocks and the distribution of volcanism, and may provide new important indications for state of the art geodynamic models that aim to capture the evolution of magmatism and rift volcanism.

We first provide qualitative observations of the evolution of magmatism in rifts to identify commonalities among different natural settings. Then, we describe the stress model used in our simulations and the methods for computing the resulting magma trajectories. Lastly, we describe the results of our simulations, discuss implications and limitations of our model and suggest possible future directions.

2. Observations of rift magmatism

2.1. Main Ethiopian Rift

Volcanism in the Main Ethiopian Rift (hereafter MER) started prior to rift initiation, resulting in the eruption of voluminous flood basalts that erupted in two separate episodes in the areas now comprising the Ethiopian and Somalian plateaus (Fig. 1a; Bonini et al., 2005; Corti, 2009). Rifting in the Northern MER and the formation of the Afar were accompanied and followed by flood basalt volcanism inside the developing depression (Chernet et al., 1998). Subsequent volcanism was characterized by the occurrence of ignimbrites and mafic lavas inside the graben and in the proximal part of the flanks during the Mio-Pliocene (Chernet et al., 1998; Bonini et al., 2005). Then, an important phase of off-rift volcanism took place during the Pliocene, with the formation of basaltic central volcanoes on the flanks of the graben (Bonini et al., 2005). A subsequent rifting phase coincided with the deactivation of the boundary faults and the focusing of volcanism in the inner portion of the graben, as part of the transition to seafloor spreading, focusing the recent Quaternary volcanics within the axial fault system (Wonji Fault Belt; Ebinger and Casey, 2001; Bonini et al., 2005; Corti, 2009). The East African Rift System is also characterized by the presence of lower crustal sill-like magmatic intrusions: Birt et al. (1997) observed a strongly reflective lower crust directly below the Kenya Rift Graben, coherent with the presence of a high velocity underplated layer, while Mackenzie et al. (2005) explained variations in seismic reflectivity in the lower crust beneath the Main Ethiopian Rift in terms of layered sills. In addition to the lower crustal layered intrusions, Keranen et al. (2004) and Mackenzie et al. (2005) also identified a high velocity region beneath the rift axis. The latter has been interpreted as mafic intrusions feeding the magmatic centers of the rift valley through upper crustal dikes, marking a zone of focused magmatism representing a protoridge axis for future seafloor spreading (Keranen et al., 2004).

2.2. Limagne Graben, France

The Limagne Graben of the Massif Central Rift (hereafter MCR), France experienced three main rifting-related magmatic events (Fig. 1b; Michon and Merle, 2001). The first event preceded the formation of the rift basin and consisted of very scarce and scattered volcanism affecting a vast area comprising the future grabens and their surroundings. The second event immediately followed the formation of the graben and produced more than 200 monogenetic vents scattered in-rift to the North of the MCR, coinciding with the areas of pronounced crustal thinning; lastly, the major volcanic events mainly contributed to the formation of the Chaîne des Puys, the Monts Dore and Sancy stratovolcanoes and the Dèves basaltic shield, which are all located off-rift from the main graben; the more recent eruptions were also all confined to the outside of the basin. These latter major volcanic episodes were also associated with the uplift of the Massif Central, suggesting a common origin for uplift and volcanism. Michon and Merle (2001) further noticed that the development of the Eifel and the Ohře Eger rift in the Czech Republic followed a nearly identical history, with similar spatio-temporal and geochemical patterns.

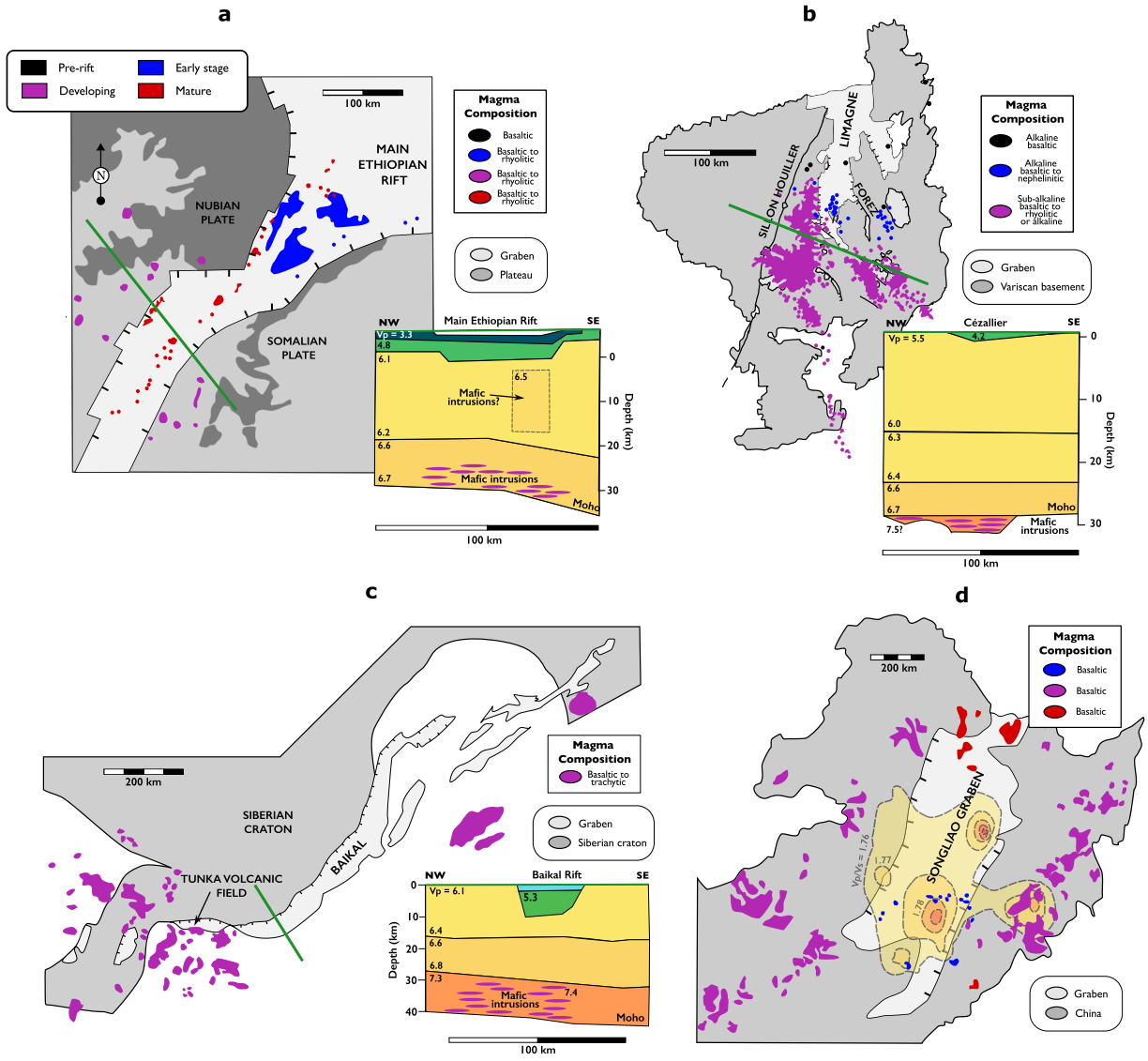

Fig. 1. a-d: Examples of spatio-temporal evolution of rift magmatism. **a**: Main Ethiopian Rift. Data on the distribution of the volcanics are adapted from Chernet et al. (1998), Bonini et al. (2005) and Maccaferri et al. (2014). Inset shows V_p crustal profile to highlight the inferred presence of lower crustal mafic intrusions, modified from Mackenzie et al. (2005). **b**: Limagne Graben of the Massif Central Rift, France. Data on the distribution of the volcanics are adapted from Michon and Merle (2001). Inset shows the V_p crustal profile, modified from Zeyen et al. (1997). **c**: Baikal Rift, Russia. Data on the distribution of the volcanics are adapted from Ivanov and Demonterova (2010). Inset shows the V_p crustal profile, modified from Thybo and Nielsen (2009). **d**: Songliao Graben, China. Data on the distribution of the volcanics are adapted from Liu et al. (2001). Inset shows contours of V_p/V_s ratio beneath the graben, with higher values interpreted to represent crustal intrusions, modified from He et al. (2014). The colors associated with each magmatic phase reflect those used for the results of our simulations (Fig. 8).

2.3. Baikal Rift, Russia

Volcanism in the Baikal Rift (hereafter BR), Russia is scarce and almost exclusively restricted to the flanks of the graben, but some volcanic centers are present in the Tunka depression (Fig. 1c; Ivanov and Demonterova, 2010). Moreover, a high seismic velocity, high reflectivity anomaly is present at depth below the rift, which Thybo and Nielsen (2009) attributed to the presence of multiple strong reflectors in the lower crust, interpreted to be horizontal sill-like magmatic intrusions. These intrusions would isostatically compensate the formation of the graben, explaining the lack of crustal thinning observed in the same area.

2.4. Songliao Graben, China

Volcanism in the Songliao Graben (hereafter SG), China commenced in the late Cretaceous with eruption of basalts scattered across the graben floor and on limited portions of the eastern flank (Fig. 1d; Liu et al., 2001). From 39 to 1.5 Ma, no volcanism has been detected inside the graben, and eruptions have focused on its eastern and western flanks, migrating progressively further from the graben (Liu et al., 2001). Lastly, the most recent eruptions (< 0.58 Ma) have clustered on the northwestern margin of the graben and on the southeastern flank of the basin. Furthermore, high V_p/V_s ratios, high V_p and regional gravity suggest the presence of mafic intrusions in the lower crust (He et al., 2014).

2.5. Summary of observations

Volcanism in rifts is observed to follow spatio-temporal patterns as the rift evolves (Fig. 2). Volcanism commonly precedes rift initiation, with voluminous eruptions distributed across a large area eventually comprising the rift graben and flanks (black stripe in Fig. 2; e.g. Pasteels et al., 1989; Michon and Merle, 2001; Corti, 2009). Rifting prefer-

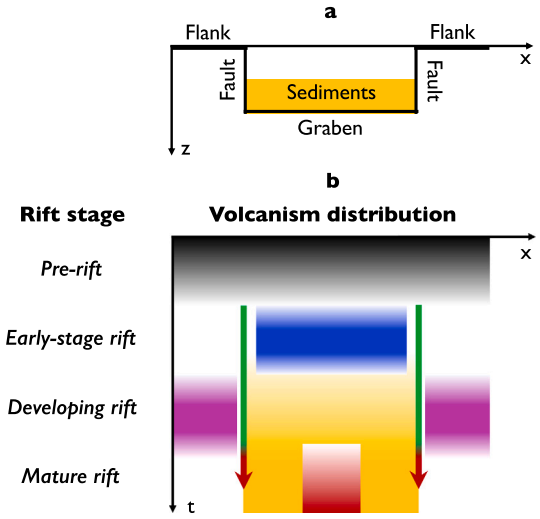

Fig. 2. Schematic summary of the observations concerning the spatio-temporal evolution of rift volcanism. **a:** Cross section of a rift showing graben, flanks, sediments and boundary faults. **b:** Timeline showing the mapview distribution of volcanism across the rift. Shaded yellow stripe represents increasing sedimentation. Green- to red-colored arrows represent the progressive deactivation of boundary faults during rift maturity. Colored stripes represent volcanism through the palette used in Figs. 1 and 8.

entially initiates in zones of inherited lithospheric weakness such as suture zones or old faults (Brune et al., 2023). As extension proceeds, deformation localizes through displacement on large boundary faults, resulting in the formation of a graben (e.g. Corti, 2009). The latter can be asymmetric (half-graben), symmetric (full-graben), or transition from one to the other during its lifetime (e.g. Baker et al., 1972). Volcanism, in turn, localizes inside the graben (blue stripe in Fig. 2; e.g. Liu et al., 2001; Michon and Merle, 2001; Corti, 2009). Prolonged extension results in the progressive downthrow of the rift graben along the boundary faults, and enhanced sedimentation due to the formation of large topographic gradients. Developed rifts are usually associated with volcanic centers punctuating the graben flanks (purple stripe in Fig. 2; e.g. Liu et al., 2001; Michon and Merle, 2001; Corti, 2009), and the accumulation of layered magmatic intrusions in the crust (Thybo and Nielsen, 2009; Thybo and Artemieva, 2013). These intrusions have been observed in a variety of extensional settings and rift zones, both active and inactive ones (Thybo and Artemieva, 2013), such as the Baikal Rift, Russia (Thybo and Nielsen, 2009), the East African Rift System (Birt et al., 1997; Mackenzie et al., 2005), the Rhine Graben, Germany (Wenzel et al., 1991), the Eger Rift, Central Europe (Hrubcová et al., 2017) the North American Midcontinent Rift (Hinze et al., 1992), the Donbas Basin, Ukraine (Lyngsie et al., 2007) and the Songliao Graben, China (He et al., 2014). Lastly, some rifts achieve maturity, accompanied by the deactivation of the boundary faults and the localization of volcanism and deformation in the axial portion of the graben (e.g. Corti, 2009). This marks the transition to oceanic spreading (e.g. Ebinger and Casey, 2001). Although the transitions between the so defined phases of magmatic activity occur on much shorter timescales if compared to the overall duration of rift volcanism, overlap between different stages is often observed. Changes in melt availability between melt-poor and melt-rich rifts impact the abundance of volcanism but seem to have no effect on their patterns.

3. Modeling magma propagation in rifted areas

Physics-based models of magma pathways in brittle-elastic rock may be broken down into two separate components (e.g. Neri et al., 2018; Rivalta et al., 2019):

i) A model for the stress state of the Earth's crust or lithosphere. The stress tensor at each point in space and time is calculated superposing the relevant stress inducing mechanisms, such as gravitational loadings/unloadings, confining and tectonic stresses, and the stresses induced by previous intrusions. The stress tensor is then diagonalized at every point in space to obtain the principal stresses (σ_1, σ_2, σ_3 from most compressive to least compressive) and their orientations. Here we define the vectorial field $\vec{v}_3$ as having at every point in space the same orientation as the eigenvector associated to σ_3 and directed towards the direction where σ_3 is decreasing in magnitude.

ii) A model for the trajectories followed by magma in a given stress field. Such models define a rule for magma propagation that takes as input the elastic stress field and a starting location for a magma batch, and returns a magma pathway and an eruptive vent location should the pathway intersect the Earth's surface. The most basic model of magma trajectories was formulated by Anderson (1937). According to the Anderson theory, faults and dikes have preferred orientations in the field according to their respective dislocation modes. Faults, being shear dislocations, tend to be oriented according to the optimal shearing direction, which is at an angle with respect to the directions of the minimum and maximum principal stresses, depending on friction. In contrast, dikes, needing to open and accommodate a volume, tend to intrude perpendicular to $\vec{v}_3$. Following this principle, first-order dike pathways in plane strain configurations can be calculated as lines perpendicular to $\vec{v}_3$. This method has been used extensively in the literature (e.g. Muller and Pollard, 1977; Pollard, 1987; Roman and Jaupart, 2014; Oliva et al., 2022) and recently extended to three dimensions by Mantiloni et al. (2023). However, this model does not account for the stress induced by the dikes and by their buoyancy. Numerical models that include fracture mechanics principles (Dahm, 2000; Maccaferri et al., 2010, 2011; Davis et al., 2021) provide more insights by including these additional effects. Principal stress trajectories differ somewhat from those calculated from fracture mechanics principles (Dahm, 2000; Watanabe et al., 2002; Maccaferri et al., 2018).

3.1. A previous model for off-rift volcanism

Maccaferri et al. (2014) simulated magma propagation in rifts through the boundary element dike propagation code developed by Maccaferri et al. (2010, 2011) following Dahm (2000). They modeled the state of stress of rift zones by applying a uniform strip-unloading of width W on the free surface of a half-space, simulating the creation of the rift graben. A similar approach based on gravitational unloading had been previously used to model icecap melting (Hooper et al., 2011) and caldera formation (Corbi et al., 2015; Rivalta et al., 2019). The resulting stresses in the elastic half-space are (e.g. Jaeger et al., 2009):

$$\sigma_{zz} = \frac{P}{\pi}[(\theta_1 - \theta_2) - \sin(\theta_1 - \theta_2)\cos(\theta_1 + \theta_2)] \quad (1)$$

$$\sigma_{xx} = \frac{P}{\pi}[(\theta_1 - \theta_2) + \sin(\theta_1 - \theta_2)\cos(\theta_1 + \theta_2)] \quad (2)$$

$$\sigma_{xz} = \frac{P}{\pi}[\sin(\theta_1 - \theta_2)\sin(\theta_1 + \theta_2)], \quad (3)$$

where θ_1 and θ_2 are shown in Fig. 3a, together with the geometry of the system, $P = \rho g D$ is the unloading pressure, ρ is the crustal density, g the acceleration due to gravity and D the basin depth. A uniform stress σ_{tec} was superimposed to simulate tectonic extension.

Maccaferri et al. (2014) found that dike trajectories in this problem are controlled by the ratio $K = \pi\sigma_{\text{tec}}/2P$ between the tectonic stress and the unloading pressure: their competition regulates the rotation of the directions of the principal stresses, which in turn controls the curvature of magma pathways since dikes propagate roughly perpendicular to the local direction of least compression $\vec{v}_3$. In particular, when the unloading pressure dominates over the tectonic stretching, $\vec{v}_3$ becomes vertical or sub-vertical over a depth interval under the graben. The condition for which $\vec{v}_3$ is vertical along the z axis is obtained by requiring that (Maccaferri et al., 2014):

$$\sigma_{zz}(x = 0, z) > \sigma_{xx}(x = 0, z) + \sigma_{\text{tec}} \quad (4)$$

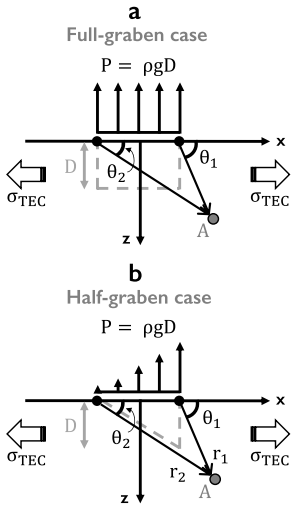

Fig. 3. Geometries used for the calculation of stresses in the full-graben (**a**) and the half-graben (**b**) cases. Symbols refer to the unloading formulation described in sections 3.1 and 3.3.

since the shear stresses σ_{xz} are null in $x = 0$ (eq. (3)). Substituting eqs. (1) and (2) in eq. (4), they found that when $K < 1$ the stress barrier is located at depth

$$z_1 < z < z_2 \tag{5}$$

where

$$z_1 = \frac{W}{2}\frac{1-\sqrt{1-K^2}}{K}, \quad z_2 = \frac{W}{2}\frac{1+\sqrt{1-K^2}}{K}. \tag{6}$$

As a consequence, dikes ascending from below z_1 are deflected from their vertical path, and if voluminous enough to escape the stress barrier end up reaching the surface outside the graben. Maccaferri et al. (2014) termed 'stress barrier' the region between z_1 and z_2 where $\vec{v}_3$ is subvertical.

3.2. Evolution of rift stresses through time

Here, we extended the model of Maccaferri et al. (2014) to a time-dependent problem. We employed a plane strain assumption and modeled a deepening rift through a gradually increasing strip unloading (eqs. (1)-(6)). The strip unloading formulation has the advantage of keeping the model simple and transparent and not relying on too many parameters, facilitating the interpretation of results. A comparison of the stresses resulting from eqs. (1), (2) and (3) and numerical boundary element calculations accounting for the contribution of the shape of the free-surface to the gravitational stresses show that for the geometries relevant here the stress models are similar both in terms of orientation and intensity of the principal stresses (Fig. S1); this confirms that the analytical unloading formulas in plane strain are adequate for calculating at zero-order the stress induced by a simplified graben geometry. Rift basin length along their axis generally exceeds their width and depth by at least an order of magnitude, motivating our plane strain assumption, which therefore applies to the central parts of the basins and breaks down close to their extremities. In order to explore more complex geometries, or the behavior of dikes propagating close to the far ends of the basins or along their length, more elaborate 3-D models need to be used (e.g. Davis et al., 2021).

For simplicity, we assumed that the unloading width W remains constant throughout most of the rifting process and that the rift deepens at a constant deepening rate α, so that D evolves as $D = \alpha t$. This approximation is supported by evidence suggesting that the width of narrow rifts is acquired early in their lifetime and does not reflect their age, making fault downthrow and sediment infill better indicators of rift maturity (Modisi et al., 2000).

The time dependent unloading pressure is therefore given by:

$$P(t) = \rho g D(t) = \rho g \alpha t, \tag{7}$$

where P at a given time t is the result of the cumulative downthrow D of the graben up to time t. In other words, it is the existence of the graben that generates the stresses, rather than its deepening velocity.

Substituting eq. (7) in eqs. (6) we obtained two equations for the time dependence of the upper and lower depth of the stress barrier:

$$z_1 = \frac{W}{\pi}\frac{\rho g \alpha t}{\sigma_{tec}}\left(1-\sqrt{1-\left(\frac{\pi}{2}\frac{\sigma_{tec}}{\rho g \alpha t}\right)^2}\right) \tag{8}$$

$$z_2 = \frac{W}{\pi}\frac{\rho g \alpha t}{\sigma_{tec}}\left(1+\sqrt{1-\left(\frac{\pi}{2}\frac{\sigma_{tec}}{\rho g \alpha t}\right)^2}\right). \tag{9}$$

The evolution of the stress barrier is shown in Fig. 4 for several values of rift width W. We will use these results as an aid to understand our numerical simulations for the full-graben case (see sections 3.4 and 4.1).

3.3. Half-graben

Half-grabens can be modeled in a similar way to full grabens by considering unloading strips shaped as right triangles (Fig. 3b). The resulting stresses in a half-space are (Jaeger et al., 2009, note that here we have fixed a sign mistake):

$$\sigma_{zz} = \frac{P}{2\pi}[[1+(x/b)](\theta_1-\theta_2)-\sin(2\theta_1)], \tag{10}$$

$$\sigma_{xx} = \frac{P}{2\pi}[[1+(x/b)](\theta_1-\theta_2)+\sin(2\theta_1)-(2z/b)\ln(r_2/r_1)], \tag{11}$$

$$\sigma_{xz} = \frac{P}{2\pi}[1-(z/b)(\theta_1-\theta_2)+\cos(2\theta_1)], \tag{12}$$

where $b = W/2$ and θ_1, θ_2, r_1 and r_2 are shown in Fig. 3b.

We determined the stress barrier by finding the region where the shear stresses vanish and the direction of least compression $\vec{v}_3$ is vertical (eq. (4)), that is by solving

$$1-(z/b)(\theta_1-\theta_2)+\cos(2\theta_1) = 0 \tag{13}$$

and

$$\sigma_{zz}(x_0(z),z) > \sigma_{xx}(x_0(z),z) + \sigma_{\text{tec}}, \tag{14}$$

where $x_0(z)$ satisfies Eq. (13).

We solved eqs. (13) and (14) numerically for different values of D (i.e. for increasing time), assuming a rift deepening at a constant deepening rate α, as in the full-graben case (Fig. 5). As in section 3.2, we superimposed a uniform tectonic extensional stress σ_{tec}. We will use these results as an aid to compare our numerical simulations for a full-graben to the case of a half-graben (see sections 3.4 and 4.2).

3.4. Numerical simulations

We conducted numerical simulations to understand how the stresses generated by an evolving graben topography affect the spatio-temporal evolution of rift magmatism in rifts. To do so, (i) we modified the stress model used by Maccaferri et al. (2014) to account for the loading generated by sedimentation within the rift, (ii) and we extended the code developed by Maccaferri et al. (2011) to account for the interaction between successive dike intrusions in order to apply it to our time-dependent problem.

3.4.1. The boundary element code

In the original code, growth and propagation of an isolated crack filled with a buoyant, inviscid fluid is calculated for any given stress

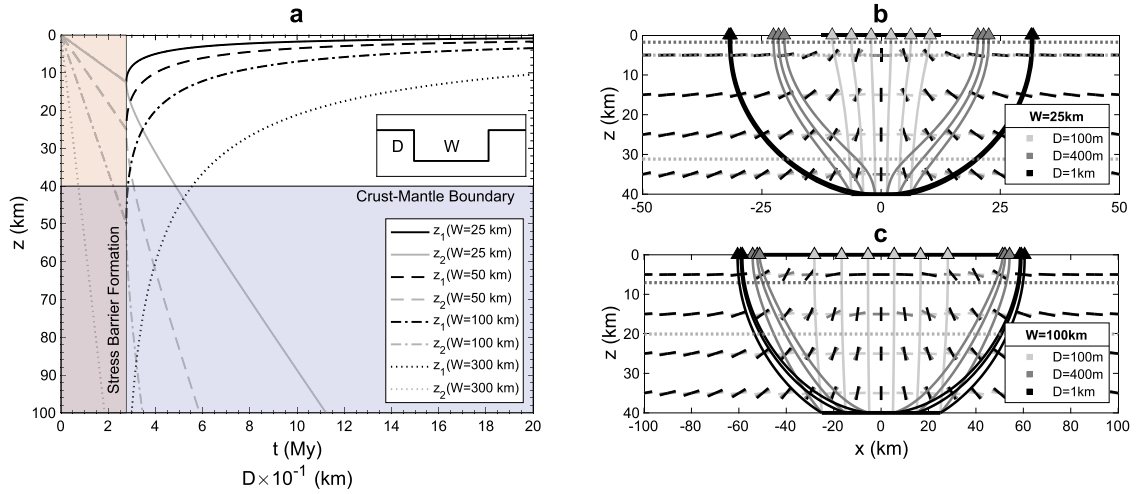

Fig. 4. a: Evolution of the stress barrier: z_1 (black) and z_2 (gray) for a full-graben deepening at a rate of $\alpha = 1 \times 10^{-4}$ m/y, plotted with respect to time for graben widths $W = 25$, 50, 100 and 300 km. Figure is colored in blue below the chosen depth of the Moho $z_{\text{Moho}} = 40$ km. Figure is colored in red up to the critical depth (or time) of stress barrier formation. Inset shows the geometry of the unloading. **b-c**: Directions of least compression (short segments), dike trajectories (curved lines) and surface arrivals (triangles) in a $W = 25$ km (**a**) and a $W = 100$ km (**b**) wide full-graben for $D = 100$ m (light gray), $D = 400$ m (dark gray) and $D = 1$ km (black). A uniform horizontal tensional stress $\sigma_{tec} = 5$ MPa is superimposed to the unloading stresses. Horizontal lines represent the upper and lower limits of the stress barrier. Black bold segments at $z = 0$ km and $z = 40$ km represent the extent of the rift and the magma ponding zone, respectively.

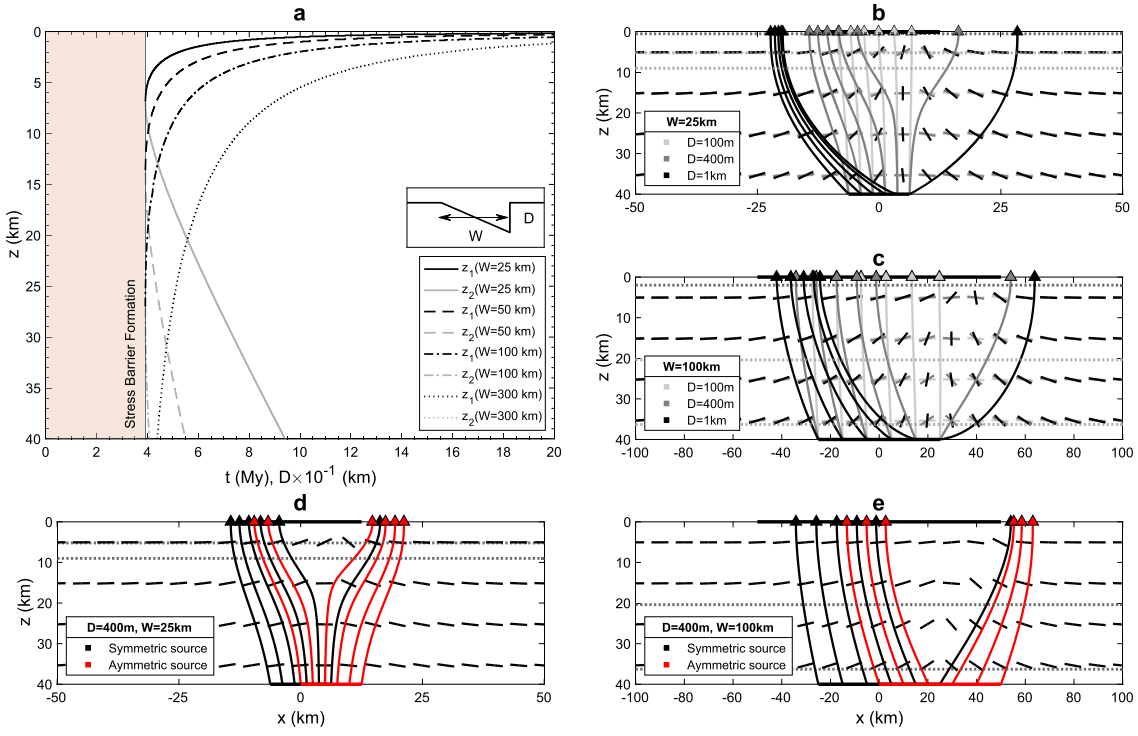

Fig. 5. a: Evolution of the stress barrier for a half-graben: z_1 (black) and z_2 (gray) for a full-graben deepening at a rate of $\alpha = 1 \times 10^{-4}$ m/y, plotted with respect to time for graben widths $W = 25$, 50, 100 and 300 km. Figure is colored in blue below the chosen depth of the Moho $z_{\text{Moho}} = 40$ km. Figure is colored in red up to the critical depth (or time) of stress barrier formation. Inset shows the geometry of the unloading. **b-c**: Directions of least compression (short segments), dike trajectories (curved lines) and surface arrivals (triangles) in a $W = 25$ km (**a**) and a $W = 100$ km (**b**) wide half-graben for $D = 100$ m (light gray), $D = 400$ m (dark gray) and $D = 1$ km (black). **d-e**: Directions of least compression (short segments), dike trajectories (curved lines) and surface arrivals (triangles) in a $D = 400$ m deep, $W = 25$ km (**d**) and $W = 100$ km (**e**) wide half-graben for a symmetric (black bold lines and triangles) and an asymmetric (red bold lines and triangles) ponding zone. A uniform horizontal tensional stress σ_{tec} is superimposed to the unloading stresses. Horizontal lines represent the upper and lower limits of the stress barrier. Black bold segments at $z = 0$ km and $z = 40$ km represent the extent of the rift and the magma ponding zone, respectively.

field. The dike is modeled as a mixed mode crack, made of a set of contiguous and interacting dislocations. The stress boundary conditions are provided by i) the magma overpressure, which is the difference between the magma pressure and the confining stress, the latter resulting from the superposition of lithostatic pressure and the normal components of topographic or tectonic stresses; and ii) the shear stress due to any tectonic stress or topographic load. The trajectory of the dike is determined by adding a new dislocation ahead of the crack tip, testing different orientations and selecting that which maximizes the sum of strain and gravitational energy release (Griffith, 1921; Dahm, 2000). The emplacement of dikes at depth modifies the local stress field: propagation of dikes in the proximity of previously emplaced ones results in focusing and crossing of dikes (Ito and Martel, 2002; Kühn and Dahm, 2008). We model dike interaction by updating the background stress field for subsequent simulations superposing the stress field produced by previously emplaced dikes. Dikes that reach the surface of the modeled half-space are assumed to erupt, their stress field is not considered in the following computations.

The effective unloading pressure at any time is given by

$$P_{\mathrm{eff}}(t) = g[\rho D(t) - \rho_s T(t)] \tag{15}$$

where ρ_s is the density of the sediments.

3.4.2. Model parameters and setup

We assumed the background state of stress σ^b to be lithostatic, so that $\sigma^b_{xx}(z) = \sigma^b_{zz}(z) = \rho g z$ and we superimposed to the unloading stresses calculated from eqs. (1), (2) and (3) a uniform tectonic extensional stress $\sigma_{\mathrm{tec}} = 5$ MPa, in line with the choice of Maccaferri et al. (2014). Regional and tectonic stresses in the crust and lithosphere build up until they match the stresses at which rock is expected to yield. Previous works have estimated the total force exerted by tectonic processes (ridge push, slab pull) on the lithosphere to be approximately $1-4$ TN m^{-1} (e.g. Forsyth and Uyeda, 1975; Kusznir, 1991), and this has been repeatedly assumed to represent the strength of the lithosphere (Liu and Zoback, 1997; Zoback and Townend, 2001). For a lithospheric thickness of 100 km, this would imply a strength of $10-40$ MPa. Laboratory experiments and numerical models have constrained the strength of cratonic lithosphere to be of the order of 100 MPa (Kohlstedt et al., 1995; Mallard et al., 2016). However, rifting initiation preferentially occurs along lithospheric suture zones where continents collided during previous stages of the Wilson cycle (Brune et al., 2023). For instance, this is the case for the Afro-Arabian Rift System (Corti, 2009), the Baikal Rift (Logatchev and Zorin, 1992) and the Massif Central Rift (Faure et al., 2009). Suture zones are much different from those of cratons due to inherited weaknesses and the presence of a thickened and hotter crust, with the net result of making them weaker and therefore preferential sites of strain localization (Brune et al., 2023). In fact, the strength of suture zones is considered to be at least a factor of 10 less than that of cratons (Hyndman et al., 2005), resulting in yield stresses of the order of 10 MPa, as applied by previous numerical models (Dang et al., 2020). This is a factor of 2 greater than our chosen parameter. However, the key parameter in our models is not the extensional stress itself, but the ratio $K = \pi\sigma_{\mathrm{tec}}/2P$ between the latter and the unloading pressure (Fig. 6). Consequently, higher tectonic stresses can result in the same pattern provided that K stays constant (that is if deeper basins are considered), which is the case for many existing rifts. For instance, the Limagne graben of the French Massif Central Rift is at least 3 km deep, grabens in the Main Ethiopian Rift and in the Kenya Rift are up to 5 km deep, while the Baikal Rift graben reaches depths of 10 km.

We conducted 20 sets of simulations for a $W = 100$ km wide full graben (Fig. 8). All the physical parameters employed in the simulations are listed in Table 1. During the first 10 sets the graben deepens from $D = 100$ m to $D = 1$ km at steps of 100 m each. For the remaining 10 sets, we account for the role of sedimentation through the superposition of a strip loading increasing from a thickness of $T = 100$ m to $T = 800$ m, reflecting the progressive leveling of topographic gradients in rifts

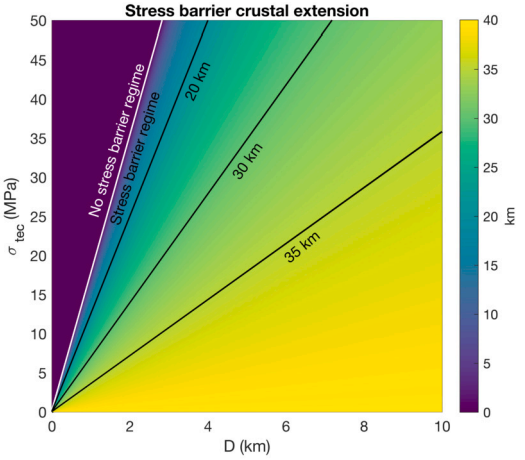

Fig. 6. Extension of the stress barrier in a 40 km deep crust as a function of basin depth D and tectonic extensional stress σ_{tec}. White line represents the transition from the "no stress barrier regime" to the "stress barrier regime". Black lines are isopleths of stress barrier crustal extension.

operated by sedimentation. For simplicity, during sedimentation, the basin depth was kept fixed at $D = 1$ km, simulating the deactivation of the boundary faults during rift maturity. This assumption has the advantage of isolating the effect of sedimentation, favoring a clearer interpretation of the results of our idealized model. In reality, graben deepening and sedimentation rates are expected to proceed in parallel during rift evolution and are not expected to be entirely independent.

After each deepening/sedimentation step, we injected a group of dikes (ranging from 4 during the first sets to 8 during the last) from depth and let them propagate until they either reached the surface or stalled. Each dike was injected after the propagation of the previous dike had ceased. If the dike reaches the surface, it is assumed to erupt, and its stress field is not considered in the computation of the background stress for the subsequent dikes. If the dike stalls in the crust, we add the stress field generated by the dike after its emplacement to the background stress, and let the following dikes propagate in the updated stress field. A flow chart illustrating the numerical simulations is provided in Fig. 7.

Each injected dike has a magma density at atmospheric pressure of 2600 kg/m^3. Less buoyant magmas would require more volume to propagate (Weertman, 1971; Secor and Pollard, 1975). For the first sets of simulations, dikes were injected from a depth representing the crust-mantle boundary ($z_{\mathrm{inj}} = z_{\mathrm{Moho}} = 40$ km). Over the suite of simulations, we increased the number of injected dikes to represent intensified melting due to decompression of the asthenosphere, and we progressively changed the injection depth z_{inj} following the emplacement of progressively shallower crustal intrusions that can act as new locations of dike nucleation ($z_{\mathrm{inj}} < z_{\mathrm{Moho}}$). The horizontal injection coordinate x_{inj} was also progressively changed to reflect higher probabilities of dike nucleation from areas of higher sill density. Detailed input parameters for the model setup of each set of simulations, including basin depth, sediments thickness, and starting location of every dike are provided in Table S1.

4. Results

4.1. Time evolution of rift volcanism

From our simulations, we identify four main stages in the development of rift-related volcanism:

i) Early in-rift volcanism: as long as $D < D_c = \pi\sigma_{tec}/2\rho g\alpha$, the basin is not deep enough for a stress barrier to form and the real parts of eqs. (8) and (9) coincide (Fig. 4a). During this regime the direction of least compression is roughly horizontal everywhere below the graben (Fig. 4c), so that dikes ascend sub-vertically towards the surface of the

Table 1
Values of the parameters employed in the simulations.

Symbol	Definition	Value or range	Unit
D	Basin depth	0-1000	m
D_c	Basin depth at stress barrier formation ($D_c = \pi\sigma_{tec}/2\rho g$)	280	m
g	Gravitational acceleration	9.81	m·s^{-2}
K	Magma bulk modulus	10	GPa
l	Initial dike length	5	km
l_0	Elementary dislocation length	0.1	km
P	Unloading pressure ($P = \rho g D$)	28	MPa
T	Sediment thickness	0-800	m
t_c	Time at stress barrier formation ($t_c = \pi\sigma_{tec}/2\rho g\alpha$)	2.8	Myr
V	Dike cross-sectional area	0.0075	km^2
W	Graben width	25, 50, 100	km
α	Graben deepening rate	1×10^{-4}	m·yr^{-1}
ρ_m	Magma density	2600	kg·m^{-3}
z_1	Upper limit of the stress barrier	-	m
z_2	Lower limit of the stress barrier	-	m
z_{inj}	Dike injection depth	40-24	km
z_{Moho}	Crust-Mantle boundary depth	40	km
ρ_m	Magma density	2600	kg·m^{-3}
μ	Rock rigidity	20	GPa
ρ	Rock density	2900	kg·m^{-3}
ρ_s	Sedimentary layer density	2700	kg·m^{-3}
σ_{tec}	Extensional uniform tectonic stress	5	MPa

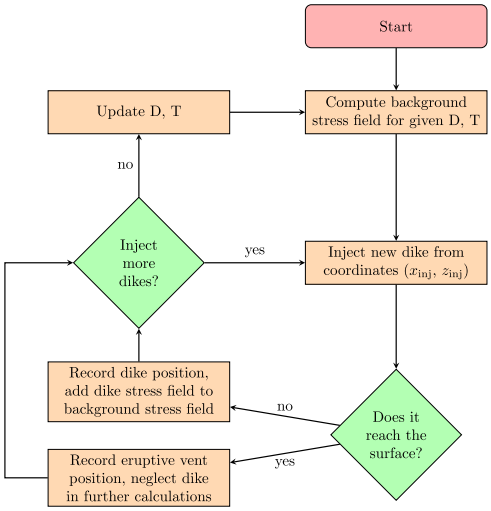

Fig. 7. Flow chart illustrating the workflow of the numerical simulations.

basin (Fig. 8a). Trajectories tend to diverge from each other so that dike eruptions are scattered across the rift depression during this first stage.

ii) Off-rift volcanism and sills emplacement: as the basin deepens, the unloading pressure grows to eventually overcome the tectonic stresses, so that $\vec{v}_3$ becomes vertical under the rift in a zone bounded by z_1 and z_2, creating a stress barrier (Fig. 4). This happens for the critical depth $D_c = \pi\sigma_{tec}/2\rho g$, which is independent of rift width. In our case, this critical depth is about 280 m. Ascending dikes are deflected towards the flanks of the depression, shifting the pattern to off-rift eruptions. After the nucleation of the stress barrier, dike trajectories become increasingly more tightly spaced as the rift deepens, reducing the distance between surface arrivals and promoting the formation of a few large polygenetic volcanic edifices.

The stress barrier then broadens with time, with z_1 slowly approaching the surface while z_2 quickly descends to depth (Fig. 4a). Also, for wider rifts, or as rifts get wider, the stress barrier forms at greater depths and grows faster. This is because z_1 and z_2 scale with rift width (eqs. (8), (9)). As a consequence, the barrier already extends beneath the Moho shortly after it has formed for rifts as wide as $W = 50$ km and forms in the lithospheric mantle, in this example, for $W > 85$ km.

iii) Piling up of stacked sills and off-rift volcanism: if the stress barrier comprises the dike injection depth (i.e. if $D > \pi\sigma_{tec}/2\rho g$, and $z_{inj} > z_1$), dikes injected close to the rift axis may be deviated into horizontal sill-like structures. Due to their very limited vertical extent, they may then lack the buoyancy needed to propagate and remain trapped in the lower crust (Fig. 8b). These horizontal intrusions can in turn collect melt supplied by further injections from below and serve as magma ponding zones from where subsequent dikes are nucleated. This way, progressively shallower horizontal intrusions form, promoting the stacking of the sills under the rift (Fig. 8c).

iv) Late in-rift volcanism: over long time scales the stacked sills may intrude thick portions of the crust so that z_{inj} approaches z_1. Concurrently, in our simulations, the sedimentation rate exceeds the deepening rate, reflecting deactivation of the boundary faults during rift maturity. As a result, the loading due to the accumulation of sediments progressively compensates the unloading induced by the excavation of the rift, causing z_1 to deepen and eventually overcome z_{inj}. When z_{inj} coincides with z_1, the shallowest possible sill is created at a depth of about z_1. Above this depth, the direction of least compression is horizontal again so that dikes injected from the sill at the top of the pile erupt inside the rift basin. The combined effect of the shallowing of the injection depth due to sill stacking and the deepening of the stress barrier due to sedimentation, thus, promotes a later stage where volcanism shifts back to the inside of the rift (Fig. 8d). A dike nucleating from this shallow depth is expected to be oriented vertically (see orientation of principal stresses above z_1 in Fig. 4b) and propagate laterally along the rift axis. Thus, stress-driven dikes in this phase may dislocate at once the entire layer of crust above the stacked sills and create the conditions for more focused crustal splitting and dike propagation, representing a shift from continental rifting to incipient oceanic spreading.

4.2. Comparison with a half-graben

Half-grabens require a larger basin depth to develop a stress barrier, and for a given graben depth, a half-graben stress barrier locates at a shallower depth, if compared to a full-graben (Figs. 4a and 5a). The first of these differences has the effect of extending the period of time during which there is no stress barrier, promoting a longer phase of monogenetic scattered volcanism inside the rift basin. The second difference, in turn, results in prolonging the time (and depth) interval for which $z_1 < z_2 < z_{Moho}$, favoring dike ascent and reducing the likelihood of sill formation.

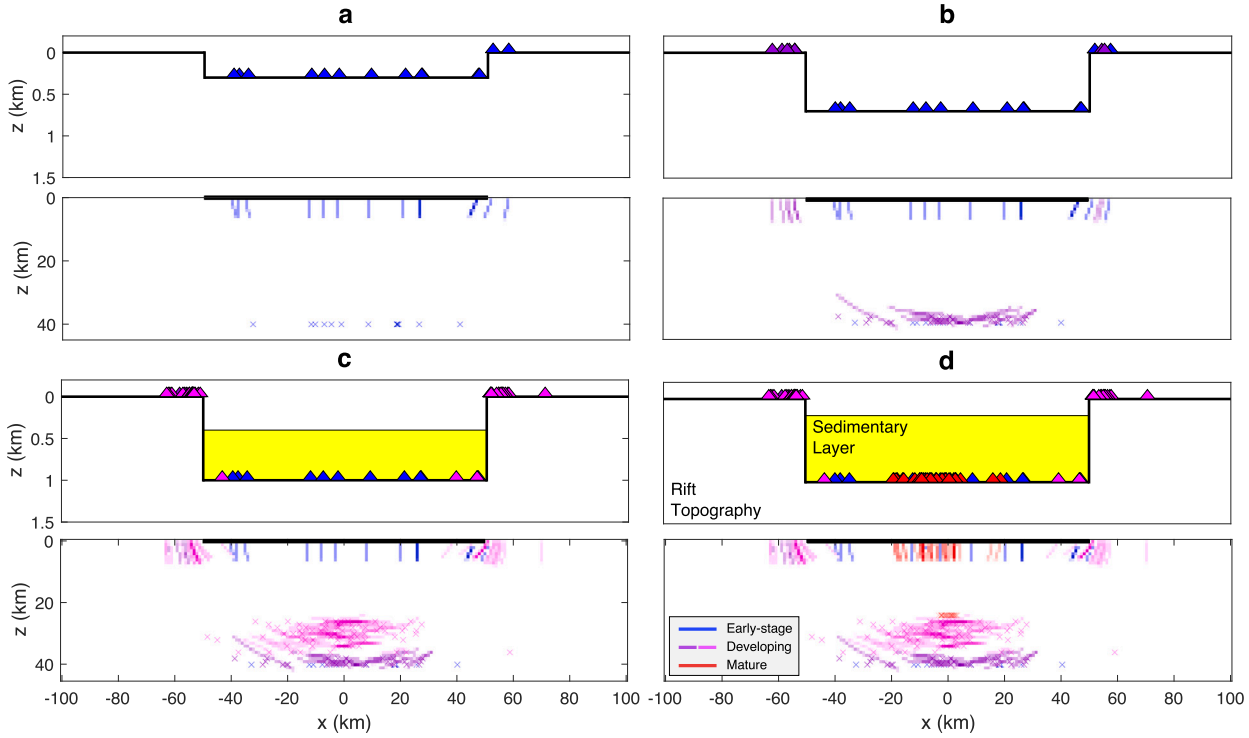

Fig. 8. a-d: The four stages of rift-related volcanism identified in our simulations. **a**: Early scattered in-rift volcanism. **b**: Off-rift volcanism and sill formation. **c**: Sill stacking and off-rift volcanism. **d**: Late axial in-rift volcanism. *Upper panels*: Bold line represents rift topography. Sedimentary layer is patched in yellow. Colored triangles mark the locations of surface dike arrivals. *Lower panels*: Density plots of dike emplacements. Colored crosses indicate the coordinates at which dikes are injected.

The shear stresses σ_{xz} for a rectangular basin are null only for $x = 0$, so that the stress barrier sits below the rift axis (Maccaferri et al., 2014). The stress barrier for the half-graben has a different shape, being shifted to the right of $x = 0$ and deflected towards the deeper side of the graben (Fig. 5). The main consequence is that dike trajectories are no longer symmetrical with respect to $x = 0$. Assuming that dikes are injected from a horizontal strip of length W/2 centered at $x = 0$ (as in the full graben case), this results in more concentrated paths on the negative x direction. The resulting volcanism would therefore tend to focus on the left side of the half-graben, that is its shallowest part (Fig. 5d,e). However, magma trajectories and the resulting surface arrivals for a half-graben are strongly sensitive to the horizontal coordinate at which dikes nucleate: dikes injected from below the shallower side of the basin may still erupt within the rift, while those that form under the deeper side tend to ascend towards the flank. If the deep magma ponding zone is shifted towards the deeper side (e.g. in a hypothesis where the decompression due to the graben formation contributes to melting) more trajectories will come from the deeper side of the basin, favoring off-rift arrivals or even one-sided volcanism (Fig. 5d,e).

As the barrier grows both in extension and intensity, surface volcanism becomes less scattered and tends to concentrate in narrower areas, as was also observed in the full-graben case. In this case, however, the presence of the stress barrier does not hinder the possibility of in-rift volcanism on the shallower side of the basin, even for high values of basin depth D.

5. Discussion

We showed that as a deepening rift graben progressively decompresses the crust and lithosphere, decompression is accompanied by a gradual rotation of crustal stresses. If the graben becomes deeper than a critical depth, the magnitude of the stress rotation can be locally so large that the most and least compressive stress directions may switch. Since magma pathways are predominantly steered following the orientation of principal stresses, a deepening rift may be associated with significant shifts in the distribution of surface vents and in the architecture of crustal intrusions, with a predominantly vertically-organized fabric switching to underplating.

The same principles that we employed in our work have been used with growing success to estimate the propagation pathways of magma at the volcano scale in several different settings (e.g. Hooper et al., 2011; Roman and Jaupart, 2014; Sigmundsson et al., 2015; Rivalta et al., 2019). This further supports our simple model.

On the basis of the success of this extremely simplified approach (compared to the complexity and number of parameters of a geodynamic model) we propose that the main features of magmatism and volcanism in rifts and elsewhere can be reproduced by accounting for a few factors: 1) elasticity (as described by Hooke's law), 2) gravitational stresses due to redistribution of surface loads during rift development, 3) dike-dike interactions, 4) physically sound magma pathways calculations that consider dikes as opening fractures, thus aligning perpendicular to $\vec{v}_3$. We propose that incorporating our approach into geodynamic models will allow to better constrain how much and where melt volumes are available and the evolution of magma properties, and developing comprehensive geodynamic simulations able to reproduce the main features of magmatism and volcanism. This would in turn provide a way of estimating poorly constrained rifting parameters such as tectonic stresses, which cannot be directly determined (e.g. by using the inversion approaches proposed by Rivalta et al., 2019), and applying our model to specific case studies.

5.1. Comparison with nature

The broad-scale magmatism and volcanism patterns usually observed during rift evolution are consistent with our simple analytical stress model, which has only three parameters. The early-stage flankward migration of volcanism is typical of several rifted areas, such as the Main Ethiopian Rift (Chernet et al., 1998; Bonini et al., 2005), the

Massif Central Rift (Michon and Merle, 2001) and the Songliao Graben (Liu and Zoback, 1997). In our model, the shift occurs once a critical basin depth is reached, which depends on the tectonic extensional stress and the density of the crustal rocks. The current available data do not allow to prove the existence of such a critical depth, but future work can focus on estimating this quantity for rifts of different nature.

The emplacement of stacked, sub-horizontal sills in the lower crust or lithospheric mantle is observed ubiquitously across a large number of rift settings (Thybo and Artemieva, 2013). In our model, this is a consequence of the stress barrier extending below the dike injection depth, and the resulting shallowing of the injection depth as magma progressively pools at shallower levels. This may eventually result in dikes nucleating above the stress barrier created by rift unloading and erupting in the axial part of the graben. The inward migration of volcanism associated with this last phase is commonly observed in more mature rifts (such as the MER), where it is crucial in assisting the transition to seafloor spreading (e.g. Corti, 2009; Ebinger and Casey, 2001).

While some features of rift magmatism (such as the presence of off-rift volcanoes and stacked sills in the middle-lower crust) are common to all the natural settings shown in this work, others are not. For example, while the MER, the MCR and the SG all exhibit an early flankward migration of volcanism, the BR is mostly characterized by off-rift volcanism, with limited amount of in-rift volcanics. Moreover, both the SG and the MER showcase a late-stage riftward migration of volcanism, but the MCR and the BR do not. The model described in this paper is intended not only to provide a framework to explain the commonalities between natural settings, but also to account for possible differences once the model will be applied in more detail to specific case studies.

5.2. The impact of tectonics

The evolution of rift volcanism has been often explained in terms of the impact of tectonics on rifting. Frequent explanations argue that as deep-reaching boundary faults are established, they would channelize the ascending magma and lead to the creation of large volcanoes close to the fault margins (Bosworth, 1987; Ebinger, 1989; Corti et al., 2004). Indeed, off-axis volcanoes are often aligned to the boundary faults, suggesting a connection. However, eruptive centers are most frequently located on the footwall of the boundary faults and, thus, clearly offset from the suggested magma pathway. The graben-unloading model offers a simple explanation of the alignments: the establishment of a graben topography leads magma trajectories starting from the crust-mantle boundary to converge just off-rift (Maccaferri et al., 2015; Neri et al., 2018). In the model presented here, we clarify that such alignments are related to the border faults reaching a critical cumulative downthrow, and are suppressed once the system of stacked sills beneath the graben reaches a critical depth.

5.3. Limitations of the model

Our model does not simulate some rifting-related processes that are usually accounted for in more complex geodynamical models. In particular, we consider only brittle-elastic rheology, which is appropriate for dike propagation, a process occurring on a short time scale of hours to weeks. Seismic evidence shows that a strong mid-lower crust is present below young rifts (Déverchère et al., 2001; Craig et al., 2011). The presence of a strong crust below rifts is also supported by topographies of wavelengths up to hundreds of kilometers lasting tens of millions of years, which imply the existence of a thick layer behaving rigidly over the same timespan (Turcotte, 1979). We note that dike propagation is a viable mechanism for magma transport also in a visco-elastic material, provided that the viscosity contrast between the rock and the magma is larger than $10^{11} - 10^{14}$, which is generally true for basaltic magmas and low-viscosity rhyolitic magmas (Rubin, 1993). In fact, magmatic underplating under continental rifts often occurs through the emplacement of sills (Thybo and Nielsen, 2009; Thybo and Artemieva, 2013), meaning that magma is still able to move by hydraulic fracturing in the lower crust. Our model does not account for the actual processes that lead to the formation of a rift graben and its sedimentary infill, which are the result of the coupled action of extension, erosion and sedimentation over million of years, while they are imposed as an input in our model. Moreover, regional tectonic stresses exert primary controls on the deepening rate of a rift, affecting in turn the rate at which rift shoulders are eroded and sediments deposited inside the graben. Since tectonic stresses can vary in space and time in rift settings, following changes in the thermal and mechanical state of the lithosphere, complex feedbacks between the structural features of a rift and its sedimentation patterns are expected to take place. However, tectonic stresses, deepening rate and sedimentation rate have been assumed to be constant and independent in our model. Future applications to specific rifts will have to account for more accurate formulations.

In our model, melt is assumed to be available from the very beginning of the rifting process. This is in reality likely true only for magma-rich rifts, while in magma-poor rifts a minimum stretching factor and, thus, graben depth would be required for melting to start. Inhibited melt production during rift initiation could result in preventing the early phase of in-rift volcanism, essentially skipping or reducing the duration of the first stage of our results but without affecting the subsequent pattern of magmatism.

Prolonged extension in rifts can result in the shallowing of the Moho due to crustal thinning (Ruppel, 1995). Alternatively, crustal thickness during extension can be maintained through the emplacement of sill-like horizontal magma bodies in the lower crust (Thybo and Nielsen, 2009; Thybo and Artemieva, 2013). In our simulations, the evolving geometry of the basin controls the emplacement of sills below the rift, which in turn is expected to control the amount of Moho uplift required to obtain isostatic equilibrium. As a result, lower crustal viscous processes such as Moho uplift are controlled top-down in our model by the shallow brittle deformation caused by graben formation, with significant implications for rifting dynamics. Implementing sound magma propagation principles in geodynamic models could help shed light on the dynamics controlling the competition between Moho uplift and the emplacement of lower crustal intrusions.

While our current model does not address the petrological aspects of rift volcanism, we expect that the different stages envisioned by our model, corresponding to different depths and timescales of stagnation of magma in the crust, should leave a detectable signature on the petrology of the erupted lavas and released gases. As an example, dike velocity is proportional to the square of the driving pressure gradient (Davis et al., 2023), so that dikes propagating at an angle δ from the vertical are a factor $\sin^2 \delta$ slower than vertically propagating dikes. This results in higher residence time of magma in the crust, with significant effects on composition that can be further scrutinized in future studies on the subject.

6. Conclusions

In spite of its simplifications, our model captures the main features of how the distribution of volcanism shifts over time while the rift matures. The main implication of our results is that the evolution of the stresses generated by a developing rift basin can account alone for the major aspects of the spatio-temporal evolution of rift magmatism. Our results imply that most of these common features may solely depend on the top-down and remote driving factors considered in our model, that is gravitational stresses due to an evolving graben topography and tectonic extension, and largely disentangled from bottom-up factors such as the mechanisms underlying rift initiation, which would still be important in determining the locations that dikes are released from. The strong connection between the structural evolution of a rift and its magmatism therefore motivates a more holistic approach in collecting data, analyzing and modeling them: joint constraints on the magmatic, tectonic and sedimentary history of rifts can help test our hypothesis, while

improvements in the model used here can make it suitable for applications to specific rifts. Further works on the topic shall also improve the stress model used here by allowing for spatially and temporally variable tectonic stresses, more complex graben geometries and crustal density structures and by including a model of the thermal evolution of the system.

CRediT authorship contribution statement

Gaetano Ferrante: Writing – original draft, Visualization, Software, Methodology, Conceptualization. **Eleonora Rivalta:** Writing – original draft, Supervision, Methodology, Funding acquisition, Conceptualization. **Francesco Maccaferri:** Writing – review & editing, Software, Methodology.

Declaration of competing interest

The authors declare that they have no known competing financial interests or personal relationships that could have appeared to influence the work reported in this paper.

Data availability

The Fortran90 code used for the numerical dike simulations and the instructions on how to compile and run the code will be made available upon request. All the data used as input for the simulations are attached as supporting information.

Acknowledgements

We are grateful to Richard F. Katz, Derek Keir and two anonymous reviewers for providing us with valuable comments that greatly improved our manuscript. This research was funded by the German Research Foundation (DFG), Grant 634756, RI 2782/2.

Appendix A. Supplementary material

A figure showing the comparison between the analytical unloading formulas used in our model and a boundary element code is provided as supplementary information, together with a table gathering the input data for the numerical simulations. Supplementary material related to this article can be found online at https://doi.org/10.1016/j.epsl.2024.118593.

References

Anderson, E., 1937. Cone-sheets and ring-dykes: the dynamical explanation. Bull. Volcanol. 1, 35–40.
Baker, B.H., Mohr, P.A., Williams, L.A.J., 1972. Geology of the Eastern Rift System of Africa, vol. 136. Geological Society of America.
Birt, C., Maguire, P., Khan, M., Thybo, H., Keller, G.R., Patel, J., 1997. The influence of pre-existing structures on the evolution of the southern Kenya Rift Valley—evidence from seismic and gravity studies. Tectonophysics 278, 211–242.
Bjorklund, T., Burke, K., Zhou, H.W., Yeats, R.S., 2002. Miocene rifting in the Los Angeles basin: Evidence from the Puente Hills half-graben, volcanic rocks, and P-wave tomography. Geology 30, 451–454.
Bonini, M., Corti, G., Innocenti, F., Manetti, P., Mazzarini, F., Abebe, T., Pecskay, Z., 2005. Evolution of the Main Ethiopian Rift in the frame of Afar and Kenya rifts propagation. Tectonics 24.
Bosworth, W., 1987. Off-axis volcanism in the Gregory Rift, East Africa: Implications for models of continental rifting. Geology 15, 397–400.
Brune, S., Kolawole, F., Olive, J.A., Stamps, D.S., Buck, W.R., Buiter, S.J., Furman, T., Shillington, D.J., 2023. Geodynamics of continental rift initiation and evolution. Nat. Rev. Earth Environ. 4, 235–253.
Chernet, T., Hart, W.K., Aronson, J.L., Walter, R.C., 1998. New age constraints on the timing of volcanism and tectonism in the northern Main Ethiopian Rift–southern Afar transition zone (Ethiopia). J. Volcanol. Geotherm. Res. 80, 267–280.
Corbi, F., Rivalta, E., Pinel, V., Maccaferri, F., Bagnardi, M., Acocella, V., 2015. How caldera collapse shapes the shallow emplacement and transfer of magma in active volcanoes. Earth Planet. Sci. Lett. 431, 287–293.
Corti, G., 2009. Continental rift evolution: from rift initiation to incipient break-up in the Main Ethiopian Rift, East Africa. Earth-Sci. Rev. 96, 1–53.
Corti, G., Bonini, M., Sokoutis, D., Innocenti, F., Manetti, P., Cloetingh, S., Mulugeta, G., 2004. Continental rift architecture and patterns of magma migration: A dynamic analysis based on centrifuge models. Tectonics 23.
Craig, T., Jackson, J., Priestley, K., McKenzie, D., 2011. Earthquake distribution patterns in Africa: their relationship to variations in lithospheric and geological structure, and their rheological implications. Geophys. J. Int. 185, 403–434.
Dahm, T., 2000. Numerical simulations of the propagation path and the arrest of fluid-filled fractures in the Earth. Geophys. J. Int. 141, 623–638.
Dang, Z., Zhang, N., Li, Z.X., Huang, C., Spencer, C.J., Liu, Y., 2020. Weak orogenic lithosphere guides the pattern of plume-triggered supercontinent break-up. Commun. Earth Environ. 1, 51.
Davis, T., Bagnardi, M., Lundgren, P., Rivalta, E., 2021. Extreme curvature of shallow magma pathways controlled by competing stresses: insights from the 2018 Sierra Negra eruption. Geophys. Res. Lett. 48, e2021GL093038.
Davis, T., Rivalta, E., Smittarello, D., Katz, R.F., 2023. Ascent rates of 3-D fractures driven by a finite batch of buoyant fluid. J. Fluid Mech. 954, A12.
Déverchère, J., Petit, C., Gileva, N., Radziminovitch, N., Melnikova, V., San'Kov, V., 2001. Depth distribution of earthquakes in the Baikal Rift System and its implications for the rheology of the lithosphere. Geophys. J. Int. 146, 714–730.
Ebinger, C., Casey, M., 2001. Continental breakup in magmatic provinces: An Ethiopian example. Geology 29, 527–530.
Ebinger, C.J., 1989. Geometric and kinematic development of border faults and accommodation zones, Kivu-Rusizi rift, Africa. Tectonics 8, 117–133.
Ellis, M., King, G., 1991. Structural control of flank volcanism in continental rifts. Science 254, 839–842.
Faure, M., Lardeaux, J.M., Ledru, P., 2009. A review of the pre-Permian geology of the Variscan French Massif Central. C. R. Géosci. 341, 202–213.
Forsyth, D., Uyeda, S., 1975. On the relative importance of the driving forces of plate motion. Geophys. J. Int. 43, 163–200.
Griffith, A.A., 1921. Vi. the phenomena of rupture and flow in solids. Philos. Trans. R. Soc. Lond., Ser. A, Contain. Pap. Math. Phys. Character 221, 163–198.
He, C., Dong, S., Chen, X., Santosh, M., Niu, S., 2014. Seismic evidence for plume-induced rifting in the Songliao Basin of Northeast China. Tectonophysics 627, 171–181.
Hinze, W.J., Allen, D.J., Fox, A.J., Sunwood, D., Woelk, T., Green, A.G., 1992. Geophysical investigations and crustal structure of the North American Midcontinent Rift System. Tectonophysics 213, 17–32.
Hooper, A., Ófeigsson, B., Sigmundsson, F., Lund, B., Einarsson, P., Geirsson, H., Sturkell, E., 2011. Increased capture of magma in the crust promoted by ice-cap retreat in Iceland. Nat. Geosci. 4, 783–786.
Hrubcová, P., Geissler, W.H., Bräuer, K., Vavryčuk, V., Tomek, Č., Kämpf, H., 2017. Active magmatic underplating in western Eger Rift, central Europe. Tectonics 36, 2846–2862.
Hyndman, R.D., Currie, C.A., Mazzotti, S.P., 2005. Subduction zone backarcs, mobile belts, and orogenic heat. GSA Today 15, 4–10.
Ito, G., Martel, S.J., 2002. Focusing of magma in the upper mantle through dike interaction. J. Geophys. Res., Solid Earth 107, ECV-6.
Ivanov, A., Demonterova, E., 2010. Extension in the Baikal rift and the depth of basalt magma generation. In: Doklady Earth Sciences. Springer Nature BV, p. 1564.
Jaeger, J.C., Cook, N.G., Zimmerman, R., 2009. Fundamentals of Rock Mechanics. John Wiley & Sons.
Janecke, S.U., Hammond, B.F., Snee, L.W., Geissman, J.W., 1997. Rapid extension in an Eocene volcanic arc: Structure and paleogeography of an intra-arc half graben in central Idaho. Geol. Soc. Am. Bull. 109, 253–267.
Keranen, K., Klemperer, S., Gloaguen, R., Group, E.W., 2004. Three-dimensional seismic imaging of a protoridge axis in the Main Ethiopian rift. Geology 32, 949–952.
Kohlstedt, D., Evans, B., Mackwell, S., 1995. Strength of the lithosphere: Constraints imposed by laboratory experiments. J. Geophys. Res., Solid Earth 100, 17587–17602.
Kühn, D., Dahm, T., 2008. Numerical modelling of dyke interaction and its influence on oceanic crust formation. Tectonophysics 447, 53–65.
Kusznir, N.J., 1991. The distribution of stress with depth in the lithosphere: thermo-rheological and geodynamic constraints. Philos. Trans. R. Soc. Lond. Ser. A: Phys. Eng. Sci. 337, 95–110.
Liu, J., Han, J., Fyfe, W.S., 2001. Cenozoic episodic volcanism and continental rifting in northeast China and possible link to Japan Sea development as revealed from K-Ar geochronology. Tectonophysics 339, 385–401.
Liu, L., Zoback, M.D., 1997. Lithospheric strength and intraplate seismicity in the New Madrid seismic zone. Tectonics 16, 585–595.
Logatchev, N., Zorin, Y.A., 1992. Baikal rift zone: structure and geodynamics. Tectonophysics 208, 273–286.
Lyngsie, S.B., Thybo, H., Lang, R., 2007. Rifting and lower crustal reflectivity: A case study of the intracratonic Dniepr-Donetsk rift zone, Ukraine. J. Geophys. Res., Solid Earth 112.
Maccaferri, F., Acocella, V., Rivalta, E., 2015. How the differential load induced by normal fault scarps controls the distribution of monogenic volcanism. Geophys. Res. Lett. 42, 7507–7512.
Maccaferri, F., Bonafede, M., Rivalta, E., 2010. A numerical model of dyke propagation in layered elastic media. Geophys. J. Int. 180, 1107–1123.

Maccaferri, F., Bonafede, M., Rivalta, E., 2011. A quantitative study of the mechanisms governing dike propagation, dike arrest and sill formation. J. Volcanol. Geotherm. Res. 208, 39–50.
Maccaferri, F., Rivalta, E., Keir, D., Acocella, V., 2014. Off-rift volcanism in rift zones determined by crustal unloading. Nat. Geosci. 7, 297–300.
Maccaferri, F., Smittarello, D., Pinel, V., 2018. On the propagation path of hydrofractures and magma-filled dykes: the competition between external stress, internal pressure, and crack length. In: EGU General Assembly Conference Abstracts, p. 8232.
Mackenzie, G., Thybo, H., Maguire, P., 2005. Crustal velocity structure across the Main Ethiopian Rift: results from two-dimensional wide-angle seismic modelling. Geophys. J. Int. 162, 994–1006.
Mallard, C., Coltice, N., Seton, M., Müller, R.D., Tackley, P.J., 2016. Subduction controls the distribution and fragmentation of Earth's tectonic plates. Nature 535, 140–143.
Mantiloni, L., Rivalta, E., Davis, T., 2023. Mechanical modeling of pre-eruptive magma propagation scenarios at calderas. J. Geophys. Res., Solid Earth 128, e2022JB025956.
Michon, L., Merle, O., 2001. The evolution of the Massif Central Rift: spatio-temporal distribution of the volcanism. Bull. Soc. Géol. Fr. 172, 201–211.
Modisi, M.P., Atekwana, E.A., Kampunzu, A., Ngwisanyi, T.H., 2000. Rift kinematics during the incipient stages of continental extension: Evidence from the nascent Okavango rift basin, northwest Botswana. Geology 28, 939–942.
Muller, O.H., Pollard, D.D., 1977. The stress state near Spanish Peaks, Colorado determined from a dike pattern. Pure Appl. Geophys. 115, 69–86.
Nakamura, K., 1977. Volcanoes as possible indicators of tectonic stress orientation—principle and proposal. J. Volcanol. Geotherm. Res. 2, 1–16.
Neri, M., Rivalta, E., Maccaferri, F., Acocella, V., Cirrincione, R., 2018. Etnean and Hyblean volcanism shifted away from the Malta Escarpment by crustal stresses. Earth Planet. Sci. Lett. 486, 15–22.
Oliva, S.J., Ebinger, C.J., Rivalta, E., Williams, C.A., Wauthier, C., Currie, C.A., 2022. State of stress and stress rotations: Quantifying the role of surface topography and subsurface density contrasts in magmatic rift zones (Eastern Rift, Africa). Earth Planet. Sci. Lett. 584, 117478.
Pasteels, P., Villeneuve, M., De Paepe, P., Klerkx, J., 1989. Timing of the volcanism of the southern Kivu province: implications for the evolution of the western branch of the East African Rift system. Earth Planet. Sci. Lett. 94, 353–363.
Pollard, D.D., 1987. Elementary fracture mechanics applied to the structural interpretation of dykes. In: Mafic Dyke Swarms, vol. 34. Geological Association of Canada, pp. 5–24.
Rivalta, E., Corbi, F., Passarelli, L., Acocella, V., Davis, T., Di Vito, M.A., 2019. Stress inversions to forecast magma pathways and eruptive vent location. Sci. Adv. 5, eaau9784.
Rivalta, E., Taisne, B., Bunger, A., Katz, R., 2015. A review of mechanical models of dike propagation: Schools of thought, results and future directions. Tectonophysics 638, 1–42.
Roman, A., Jaupart, C., 2014. The impact of a volcanic edifice on intrusive and eruptive activity. Earth Planet. Sci. Lett. 408, 1–8.
Rubin, A.M., 1993. Dikes vs. diapirs in viscoelastic rock. Earth Planet. Sci. Lett. 117, 653–670.
Rubin, A.M., 1995. Propagation of magma-filled cracks. Annu. Rev. Earth Planet. Sci. 23, 287–336.
Ruppel, C., 1995. Extensional processes in continental lithosphere. J. Geophys. Res., Solid Earth 100, 24187–24215.
Secor Jr., D.T., Pollard, D.D., 1975. On the stability of open hydraulic fractures in the Earth's crust. Geophys. Res. Lett. 2, 510–513.
Sigmundsson, F., Hooper, A., Hreinsdóttir, S., Vogfjörd, K.S., Ófeigsson, B.G., Heimisson, E.R., Dumont, S., Parks, M., Spaans, K., Gudmundsson, G.B., et al., 2015. Segmented lateral dyke growth in a rifting event at Bárdarbunga volcanic system, Iceland. Nature 517, 191–195.
Thybo, H., Artemieva, I., 2013. Moho and magmatic underplating in continental lithosphere. Tectonophysics 609, 605–619.
Thybo, H., Nielsen, C., 2009. Magma-compensated crustal thinning in continental rift zones. Nature 457, 873–876.
Turcotte, D.L., 1979. Flexure. In: Advances in Geophysics, vol. 21. Elsevier, pp. 51–86.
Watanabe, T., Masuyama, T., Nagaoka, K., Tahara, T., 2002. Analog experiments on magma-filled cracks: Competition between external stresses and internal pressure. Earth Planets Space 54, e1247–e1261.
Weertman, J., 1971. Theory of water-filled crevasses in glaciers applied to vertical magma transport beneath oceanic ridges. J. Geophys. Res. 76, 1171–1183.
Wenzel, F., Brun, J.P., Group, E.D.W., et al., 1991. A deep reflection seismic line across the northern Rhine graben. Earth Planet. Sci. Lett. 104, 140–150.
White, R., 1992. Magmatism during and after continental break-up. Geol. Soc. (Lond.) Spec. Publ. 68, 1–16.
Zeyen, H., Novak, O., Landes, M., Prodehl, C., Driad, L., Hirn, A., 1997. Refraction-seismic investigations of the northern Massif Central (France). Tectonophysics 275, 99–117.
Ziv, A., Rubin, A.M., Agnon, A., 2000. Stability of dike intrusion along preexisting fractures. J. Geophys. Res., Solid Earth 105, 5947–5961.
Zoback, M.D., Townend, J., 2001. Implications of hydrostatic pore pressures and high crustal strength for the deformation of intraplate lithosphere. Tectonophysics 336, 19–30.